Heme-binding protein CYB5D1 is a radial spoke component required for coordinated ciliary beating

Lijuan Zhao[a,b,1], Haibo Xie[c,1], Yunsi Kang[c], Yiwen Lin[a,b], Gai Liu[a], Miho Sakato-Antoku[d], Ramila S. Patel-King[d], Bing Wang[e], Cuihong Wan[e], Stephen M. King[d], Chengtian Zhao[c,f,2], and Kaiyao Huang[a,2]

[a]Key Laboratory of Algal Biology, Institute of Hydrobiology, Chinese Academy of Sciences, 430072 Wuhan, China; [b]College of Life Sciences, University of Chinese Academy of Sciences, 100039 Beijing, China; [c]Institute of Evolution and Marine Biodiversity, College of Marine Life Science, Ocean University of China, 266003 Qingdao, China; [d]Department of Molecular Biology and Biophysics, University of Connecticut Health Center, Farmington, CT 06032-3305; [e]Hubei Key Lab of Genetic Regulation and Integrative Biology, School of Life Sciences, Central China Normal University, Wuhan 430079, China; and [f]Laboratory for Marine Biology and Biotechnology, Qingdao National Laboratory for Marine Science and Technology, 266003 Qingdao, China

Edited by George B. Witman, University of Massachusetts Medical School, Worcester, MA, and accepted by Editorial Board Member Stephen T. Warren March 12, 2021 (received for review August 1, 2020)

Coordinated beating is crucial for the function of multiple cilia. However, the molecular mechanism is poorly understood. Here, we characterize a conserved ciliary protein CYB5D1 with a heme-binding domain and a cordon-bleu ubiquitin-like domain. Mutation or knockdown of *Cyb5d1* in zebrafish impaired coordinated ciliary beating in the otic vesicle and olfactory epithelium. Similarly, the two flagella of an insertional mutant of the CYB5D1 ortholog in *Chlamydomonas* (*Crcyb5d1*) showed an uncoordinated pattern due to a defect in the *cis*-flagellum. Biochemical analyses revealed that CrCYB5D1 is a radial spoke stalk protein that binds heme only under oxidizing conditions. Lack of CrCYB5D1 resulted in a reductive shift in flagellar redox state and slowing down of the phototactic response. Treatment of *Crcyb5d1* with oxidants restored coordinated flagellar beating. Taken together, these data suggest that CrCYB5D1 may integrate environmental and intraciliary signals and regulate the redox state of cilia, which is crucial for the coordinated beating of multiple cilia.

cilia | motility | redox | zebrafish | Chlamydomonas

Cilia and flagella are highly conserved organelles that project from the surface of most eukaryotic cells and perform sensory, secretory, and motile functions (1, 2). The single motile flagellum of spermatozoa propels cell body movement, whereas the two flagella of the green alga *Chlamydomonas reinhardtii* mediate oriented swimming. Coordinated beating of multiple cilia on epithelial surfaces, for example, in the trachea, oviduct, and brain ventricles of vertebrates, is crucial for mucus clearance in the airway, ovum transport in the oviduct, and cerebrospinal fluid circulation in the brain ventricles (3). Impairment of coordinated beating of these multiple cilia in humans can result in ciliopathies such as chronic respiratory problems, infertility, and hydrocephalus (4).

The beating of individual cilia/flagella depends on axonemal dyneins, which are AAA^+ enzymes that convert ATP (adenosine triphosphate) hydrolysis into mechanical force, resulting in the sliding of doublet microtubules (5). The activity of dyneins is spatiotemporally controlled by various regulatory pathways including changes in Ca^{2+}, phosphorylation, and redox state (5). Recent Cryo-EM (cryo-electron microscopy) studies have revealed that these dyneins are generally in a force-balanced state in straight axonemal regions, and that the initiation and formation of a ciliary bend by microtubule sliding may depend on an inhibitory signal that is propagated from the base-to-tip to disrupt the force-balanced state (6). To achieve coordinated beating, the activity of multiple cilia must be synchronized by both intrinsic and extrinsic factors including hydrodynamic coupling, axonemal mechanical feedback, connective structures in the basal body region, and Ca^{2+} signaling (7–10). The hydrodynamic hypothesis is supported by the observation that when two sperm or two micropipette-held somatic cells of *Volvox carteri* were placed in close proximity under hydrodynamic flow, the beating of two flagella was spontaneously synchronized (8, 10). However, multiple cilia can still maintain coordinated beating when fluid flow disappears (11), suggesting that other mechanisms are also involved.

The mechanical feedback system was proposed based on the study of light chain 1 (LCI) from *Chlamydomonas*. LC1 contains six leucine-rich repeats that form an elongated barrel (12) and binds to the microtubule-binding domain of the γ-HC (γ heavy chain) specifically (13). LC1 mutant proteins expressed in wild type *Chlamydomonas* resulted in uncoordinated flagellar beating (14). Knockdowns of LC1 in planaria also led to the loss of metachronal synchrony in the ventral cilia (7). As a conformational switch, LC1 may sense changes in axonemal curvature imposed by hydrodynamic flow and thereby modulate the activity of outer dynein arm to coordinate flagellar beating. This model is also supported by recent structural data on the LC1–γ-HC microtubule-binding domain complex (15).

Coordinated beating of algal flagella is also achieved by basal coupling through filamentary connections between basal bodies (10). These connectors control basal body alignment and cilia orientation in multiciliated cells and may also participate in coordinated beating by integrating the chemical or mechanical signals among cilia (9). However, the nature of these signals remains unknown. Ca^{2+} is a common second messenger in cilia and may also participate in coordinated beating. Knock-down of the components

Significance

Impairment of the coordinated beating of multiple cilia results in primary ciliary dyskinesia (PCD) phenotypes such as chronic respiratory problems. In this study, we find CYB5D1 is a radial spoke stalk protein that binds heme under oxidizing conditions. Mutation of CYB5D1 in zebrafish and green algae lead to uncoordinated ciliary beating. Importantly, lack of CrCYB5D1 changes the redox state of flagella. Our findings reveal the important role of redox in the coordinated beating of multiple cilia and suggest a possible PCD therapy by modulating the redox poise in cilia.

Author contributions: L.Z., C.W., S.M.K., C.Z., and K.H. designed research; L.Z., H.X., Y.K., Y.L., M.S.-A., R.S.P.-K., and B.W. performed research; S.M.K. contributed new reagents/analytic tools; L.Z., H.X., G.L., C.W., S.M.K., C.Z., and K.H. analyzed data; and L.Z., S.M.K., C.Z., and K.H. wrote the paper.

The authors declare no competing interest.

This article is a PNAS Direct Submission. G.B.W. is a guest editor invited by the Editorial Board.

[1]L.Z. and H.X. contributed equally to this work.

[2]To whom correspondence may be addressed. Email: chengtian_zhao@ouc.edu.cn or huangky@ihb.ac.cn.

This article contains supporting information online at https://www.pnas.org/lookup/suppl/doi:10.1073/pnas.2015689118/-/DCSupplemental.

Published April 19, 2021.

of the calmodulin-associated complex, such as CaM-IP2, CaM-IP3, PF6, and PCDP1, resulted in uncoordinated flagellar beating in *Chlamydomonas* (16–18). However, the coordination defect may be a secondary effect since motility-related structures such as the central pair and radial spokes exhibit structural alterations in these mutants. The two flagella of *Chlamydomonas* respond differently to changes of Ca^{2+} concentration at the low μM range, which alters flagellar coordination and results in phototactic turning (19, 20). Therefore, Ca^{2+} functions in modulating flagellar coordination during these processes.

Recent studies have shown that redox state also participates in regulating ciliary/flagellar beating in *Chlamydomonas* and mammals. The beat frequency of flagella was reduced when *Chlamydomonas* cells were treated with oxidizing agents (21). Redox poise also regulates the sign of phototaxis in *Chlamydomonas* (22). When multiple cilia on airway epithelial cells were exposed to oxidants, the mucociliary transport was inhibited (23). In addition, several redox-sensitive components have been identified in flagellar motility-related complexes, such as LC3, LC5, γ-HC, and outer dynein arm-docking complex protein 3 (DC3) in *Chlamydomonas* (24–26). Disruption of human TXNDC3 and TXNDC6, which contain modules orthologous to the thioredoxin-like LC3 and LC5 proteins in *Chlamydomonas*, results in respiratory disease (27, 28). Taken together, these findings suggest that redox plays a vital role in coordinating ciliary beating; however, the molecular mechanisms and pathways that mediate the redox response are unknown.

Here, we identify a highly conserved ciliary protein cytochrome b5-like/heme-binding domain (CYB5D1), which is required for the coordinated beating of multiple cilia in zebrafish and *Chlamydomonas.* Furthermore, our results indicate that this heme-binding protein may function in a redox signaling pathway to coordinate ciliary beating.

Results

Cyb5d1 Is a Ciliary Protein Required for Otolith Formation in Zebrafish. Using an initial whole-mount in situ hybridization and gene expression screen, we identified *cyb5d1* as a candidate ciliary gene. Zebrafish *cyb5d1* is selectively expressed in motile cilia-rich organs, including Kupffer's vesicle, otic vesicle, floor plate, pronephric duct, and olfactory placode (Fig. 1 *A* and *B*). To clarify the role of this protein during zebrafish development, we further generated a mutant allele carrying a 13 bp deletion in the target region using the CRISPR/Cas9 system (Fig. 1*C*). The *cyb5d1* mutants were able to survive to adulthood. Interestingly, mutant embryos constantly developed three otoliths in the otic vesicle at 24 hours postfertilization (hpf) and recovered to two during later development (Fig. 1 *D* and *E*). Similarly, knockdown of *cyb5d1* with morpholino oligonucleotides also produced large numbers of embryos with otolith defects (*SI Appendix*, Fig. S1 *A–D*).

Since otolith develop via the accumulation of numerous precursor particles facilitated by motile cilia movement (29), we evaluated ciliary movement in the otic vesicle using a high-speed video microscope. In wild type embryos, most cilia beat in a clockwise direction (Movie S1). In contrast, *cyb5d1* mutants displayed abnormal ciliary beat patterns, with the beating direction of some cilia changing from clockwise to counterclockwise occasionally and some cilia beating intermittently (Movie S2). Similarly, the rhythmic beating of multiple cilia bundles on the olfactory epithelia was also severely affected in *cyb5d1* morphant zebrafish (Fig. 1*F* and Movies S3 and S4). Although the beat frequency of otic vesicle motile cilia remained largely unchanged, multiple cilia displayed significantly higher beat frequency in the olfactory pit of *cyb5d1* morphants (Fig. 1 *G* and *H*). Noticeably, cilia developed normally in both the otic vesicle and olfactory pit (*SI Appendix*, Fig. S1 *E–H*), and there are no laterality defects in these mutants; the KV cilia beat normally even though *cyb5d1* is highly expressed in Kuffer's vesicle (*SI Appendix*, Fig. S1*P*). We further examined cilia development in other organs and found that the length and number of cilia were grossly normal in all tissues investigated (*SI Appendix*, Fig. S1 *I–O*). These results suggest that Cyb5d1 is essential for the coordinated beating of motile cilia, but not for cilia formation.

Deletion of *CYB5D1* in *Chlamydomonas* Causes Motility Defect. To further explore the function of CYB5D1 in ciliary motility, we used the biflagellate green alga *Chlamydomonas* as a model organism. The ortholog of CYB5D1 in *Chlamydomonas* is *FAP198* (GenBank PNM78294). *FAP198* is predicted to encode a 230 residue polypeptide (26.6 kDa) with 66% sequence similarity and 50% identity to zebrafish CYB5D1. *FAP198* hereafter is referred to as *CrCYB5D1*. CYB5D1 contains two conserved domains: a cytochrome b5-like/heme-binding domain and a cordon-bleu ubiquitin-like domain (COBL1) (*SI Appendix*, Fig. S2). From about 40,000 mutants, one putative insertional allele (*Crcyb5d1*) was obtained from an insertional mutant library (30). Sequence analyses revealed that the *AphVIII* expression cassette was inserted into the fourth exon of *CrCYB5D1* (Fig. 2*A*). A PCR product from the *Crcyb5d1* mutant was about 4.8 kb containing the 2.7 kb *AphVIII* expression cassette and 2.1 kb *CrCYB5D1* genomic DNA, which was larger than the PCR product amplified from parental strain HS211 (Fig. 2*B*). RT-PCR was also used to amplify cDNA of *CrCYB5D1* in HS211 and *Crcyb5d1*, respectively. The full-length *CrCYB5D1* coding sequence was obtained from HS211, while it was absent in the *Crcyb5d1* mutant (Fig. 2*C*). Taken together, these results confirmed that the *Crcyb5d1* mutant is functionally null for *CrCYB5D1*.

Considering that the Cyb5d1 mutation caused ciliary beating defects in zebrafish, we first determined whether cell motility was affected in the *Crcyb5d1* mutant using a 20× objective lens. Approximately, 92% of HS211 cells showed rapid directional movement (Movie S5); the swimming paths were long and smooth (Fig. 2*E*), and the average forward swimming velocity was about 161 μm/s (Fig. 2*G*). In contrast, movement was not detectable in 60% of *Crcyb5d1* cells (Fig. 2*E*) because these cells were rocking in place (Movie S6); only 40% of *Crcyb5d1* cells exhibited forward swimming, albeit, in short and kinked tracks (Fig. 2 *E* and *F*). The average forward swimming velocity was dramatically reduced to 32 μm/s in *Crcyb5d1* (Fig. 2*G*). Taken together, these results demonstrate that cell motility is severely defective in the *Crcyb5d1* mutant. The percentage of flagellated cells and the average flagellar length of *Crcyb5d1* cells were similar to HS211 (*SI Appendix*, Fig. S3 *A–C*). These results indicate that the motility defect of *Crcyb5d1* is not due to abnormal flagellar assembly.

Coordinated Flagellar Beating Is Disrupted in the *Crcyb5d1* Mutant. To further analyze the motility defect in the *Crcyb5d1* mutant, the waveform of flagellar beating was observed and recorded in real-time using a high-speed video microscope. The two flagella of most HS211 cells beat in-phase (IP state) (31, 32), in which the power stroke or recovery stroke of the two flagella coincided synchronously, resembling breaststroke swimming (Fig. 3*A* and Movie S7). The area encompassing the beat envelope of the *cis*- and *trans*-flagella was almost the same (Fig. 3 *D* and *E*), and the cell body moved forward without a change in orientation (Fig. 3*F*, box-marked line).

In contrast, the two flagella of most *Crcyb5d1* cells exhibited beating in a slip phase (Slip) (Fig. 3*B*) or antiphase state (AP) (Fig. 3*C*) (Movie S8) (31, 32). In the Slip state, when the two flagella finished the recovery stroke, the trans-flagellum began a power stroke, but the cis-flagellum was drawn back to the cell body immediately with a curled shape (Fig. 3 *B* and *D*). This flagellar beat waveform made the cell body turn in the direction of the cis-flagellum (Fig. 3*F*, round-marked line), so in the continuous Slip state, the cell body exhibited rotation in the direction of the cis-flagellum. In the AP state, while one flagellum was undergoing its

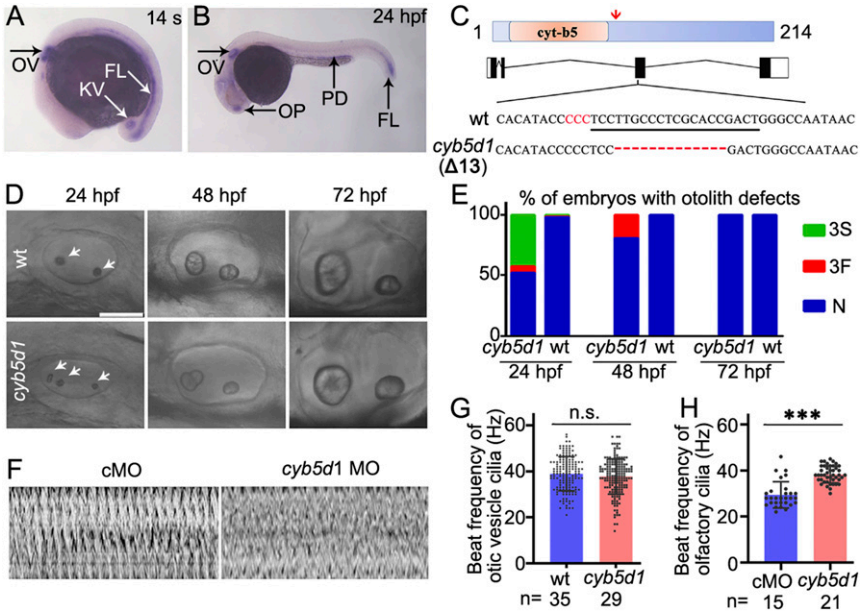

Fig. 1. Phenotypes of zebrafish *cyb5d1* mutants. (*A* and *B*) Whole-mount in situ hybridization results showing cyb5d1 expression in 14 somite (14 s) and 24 hpf embryos. OV, otic vesicle; KV, Kupffer's vesicle; FL, floor plate; PD, pronephric duct; OP, olfactory placode. (*C*) Diagram showing the protein and genomic structures of zebrafish Cyb5d1. The corresponding nucleic acid sequences of wild type (wt) and mutant alleles are shown at the bottom. The target sequence of the sgRNA is underlined, and the PAM sequence is indicated in red. Arrow points to the truncation site of Cyb5d1 in the mutant. (*D*) Phenotypes of otoliths in the OV of wt and *cyb5d1* mutants at different stages as indicated. Arrowheads indicate otoliths in the OV of 24 hpf embryos. (Scale bar, 100 μm.) (*E*) Bar graphs showing the percentage of embryos with two (normal; N) or three otoliths (three separate, 3S; three with two fused together, 3F) in different groups of embryos as indicated. Examples of embryos with 3S or 3F otoliths are shown in *SI Appendix*, Fig. S1. $n = 447$ for *cyb5d1* mutants and $n = 449$ for wild type larvae. (*F*) Kymographs showing the beating pattern of multiple cilia bundles in the olfactory pit of wild type (cMO) and *cyb5d1* morphants (*cyb5d1* MO) in 72 hpf. (*G*) Beat frequency of otic vesicle motile cilia in wild type and *cybd51* mutant embryos at the 23 somite stage. (*H*) Beat frequency of olfactory cilia in wild type (cMO) or *cyb5d1* morphants (*cyb5d1* MO) at 72 hpf. n.s., not significant; ***$P < 0.001$. Error bars are SDs for the means.

power stroke, the other one was undergoing its recovery stroke, like freestyle swimming (Fig. 3*C*). This flagellar beat waveform made the cell body rotate toward the cis-flagellum or the trans-flagellum (Fig. 3*F*, triangle-marked line). The area encompassing the beat envelope of the *Crcyb5d1* trans-flagellum was about double that of the cis-flagellum in the Slip state (Fig. 3*E*). For Slip beating observed in wild type cells, the beat frequency of the trans-flagellum is higher than that of the cis-flagellum (33); however, the Slip beating of *Crcyb5d1* is different because the beat frequency of the trans-flagellum and cis-flagellum is similar (*SI Appendix*, Fig. S6*A*).

In total, there were only 7% of Slip and 5% of AP states in the beat cycles of HS211 while 88% of beat cycles were in the IP state. In contrast, for the mutant *Crcybd51*, the percentage of Slip states increased to 48%, and AP states increased to 29% (Fig. 3*G*). The percentage of different beat states observed using a red filter was similar to that without the filter (*SI Appendix*, Fig. S4), suggesting the change of waveform in *Crcybd51* did not result from photoshock.

As nearly 90% of beating cycles in HS211 cells were in the IP state in our free-swimming cell assay, the IP state was defined as coordinated beating, and both AP and Slip states were categorized as uncoordinated beating. Using this standard, we found that about 90% of HS211 cells exhibited coordination, but in the *Crcybd51* mutant, only 20% of cells showed coordination (Fig. 3*H*). In addition, the number of nonplanar beat cycles, which occurs when flagellar beating is uncoordinated, increased in *Crcybd51* mutant compared to HS211 (*SI Appendix*, Fig. S5).

Beat frequency of the cis- and trans-flagella was the same not only in the IP and AP states but also in the Slip state (*SI Appendix*, Fig. S6*A*), suggesting that uncoordinated flagellar beating does not result from a difference in the beat frequency of the two flagella. The beat frequency of the AP state was higher than that of the IP and Slip states (*SI Appendix*, Fig. S6*A*), which makes the mean frequency of *Crcybd51* significantly higher compared to HS211 (*SI Appendix*, Fig. S6*B*). The dominance of flagella activity in demembranated and reactivated cells revealed that the trans-axoneme constantly showed dominance in *Crcybd51* cell models regardless of changes in the Ca^{2+} concentration (Fig. 3*I*). This result is consistent with the Slip waveform of *Crcybd51* in which the cis-flagellum exhibits a smaller bend envelope than the trans-flagellum (Fig. 3 *D* and *E*). Thus, a defect in the cis-flagellum resulted in the uncoordinated beating of *Crcyb5d1*.

To remove possible second-site insertions, original *Crcyb5d1* mutant was crossed with wild type strain CC124; paromomycin resistant progeny also shows the defect of coordinated flagellar beating as the original mutant (*SI Appendix*, Fig. S7). In addition, the wild type *CrCYB5D1* gene tagged with *mCherry* at the N terminus was expressed in *Crcyb5d1*. Two of the mCherry-positive strains, named *Crcyb5d1 mC::CrCYB5D1* 1# and *Crcyb5d1 mC::CrCYB5D1* 2#, were selected for further analysis. The coding sequence of mCherry-tagged *CrCYB5D1* was transcribed and translated in these two strains (Fig. 2 *C* and *D*). The swimming paths, percentage of motile cells, velocity of forward swimming, percentage of coordinated flagellar beating, and flagellar beat frequency in these two strains were similar to that of HS211 (Figs. 2 *E–G* and 3*H* and *SI Appendix*, Fig. S6*B*). Collectively, the above results confirmed that the loss of coordinated flagellar beating in the *Crcyb5d1* strain was due to mutation of the *CrCYB5D1* gene.

CrCYB5D1 Is an Axonemal Protein. To determine the localization of CrCYB5D1 in *Chlamydomonas*, the fluorescence of mC::CrCYB5D1 in *Crcyb5d1 mC::CrCYB5D1* cells was observed using 3D-SIM (three dimensions structure illumination microscopy). The mC::CrCYB5D1 exhibited a strong and continuous signal in the flagella, which was surrounded by the signal from coexpressed IFT46::YFP (Fig. 4*A*). As IFT46::YFP is a marker of the flagellar matrix and present in

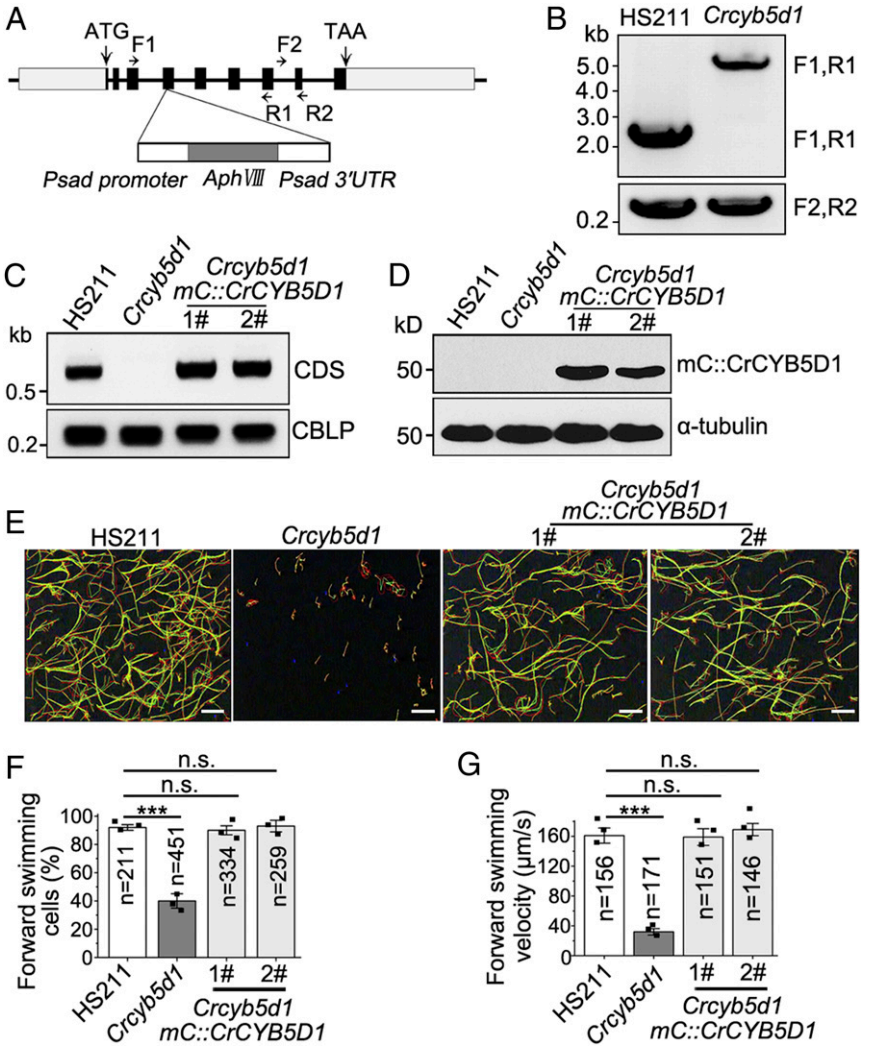

Fig. 2. CrCYB5D1 is essential for normal motility in *Chlamydomonas*. (*A*) Schematic diagram of the genomic structure of CrCYB5D1 illustrating the location of the insertion in the *Crcyb5d1* mutant. The *AphVIII* expression cassette is inserted into the fourth exon. (*B*) PCR analyses of CrCYB5D1 using genomic DNA of HS211 and *Crcyb5d1* as templates, using the primers shown in *A*. (*C*) Transcriptional analysis of *CrCYB5D1* in the indicated strains using RT-PCR. (*D*) Immunoblot of whole-cell lysates from the indicated strains using antibody against mCherry; α-tubulin served as a loading control. (*E*) The swimming tracks of individual cells from the indicated strains were recorded for a 5 s period using a micro image analyzer (Olympus). The red and green lines indicate the straight and curved motion tracks, respectively; dark blue dots are nonmotile cells. (Scale bars, 100 μm.) (*F*) Bar graph showing the percentage of forward swimming cells in the indicated strains. (*G*) The forward swimming velocity of cells in the indicated strains. For *F* and *G* the number of cells (n) measured is indicated. ***$P < 0.001$.

intraflagellar transport trains (34), this result suggested that CrCYB5D1 might be an axonemal protein. Immunoblot analysis of isolated flagella and deflagellated cell bodies of *Crcyb5d1 mC::CrCYB5D* also confirmed that CrCYB5D1 was present in the cell body and notably in the flagella, similar to the radial spoke protein RSP1 (Fig. 4*B*). When isolated flagella were separated into membrane plus matrix and axoneme fractions, CrCYB5D1 was predominately present in the axonemal fraction, similar to RSP1 but unlike the flagellar membrane protein FMG1 (Fig. 4*C*). Collectively, the above results indicate that CrCYB5D1 is an axonemal protein.

Numerous motility-related complexes are associated with the axoneme, including the central pair (CP), radial spokes (RSs), outer dynein arms (ODAs), and inner dynein arms (IDAs). To determine if CrCYB5D1 was associated with any of these complexes, the axonemes from *Crcyb5d1 mC::CrCYB5D1* were fractionated into soluble fractions and remnants using 0.6 M NaCl, and subsequently 0.5 M KI (potassium iodine) extraction. Immunoblot analysis of these fractions showed that the majority of CrCYB5D1 was resistant to NaCl extraction, but was soluble in the KI solution, similar to RSP1 and PF20 (Fig. 4*D*). Furthermore, mC::CrCYB5D1 was expressed in the *pf20* strain (lacks the central pair microtubules) (35) and in the *pf28pf30* strain (missing inner arm I1 and outer dynein arms) (36). Immunoblot analysis revealed that CrCYB5D1 was present in the flagella of both *pf20* and *pf28pf30* (Fig. 4 *E* and *F*), suggesting that CrCYB5D1 does not associate with the central pair or outer dynein arms or inner arm I1.

CrCYB5D1 Localizes to the Radial Spoke Stalk. Each radial spoke consists of a base, stalk, and head. To identify which region CrCYB5D1 associates with, mC::CrCYB5D1 was expressed in the mutant *pf17* (missing the radial spoke head) (37) and FLAG::CrCYB5D1 was expressed in the mutant *pf14* (missing the radial spoke head and stalk) (38). Both mC::CrCYB5D1 and FLAG::CrCYB5D1 can complement the mutation of *CrCYB5D1* and can be transported into the flagellum and assemble into the axoneme (Fig. 2 *C*–*G* and *SI Appendix*, Fig. S8). mC::CrCYB5D1 was present in the flagella of *pf17* (Fig. 5*A*); however, FLAG::CrCYB5D1 was absent in the

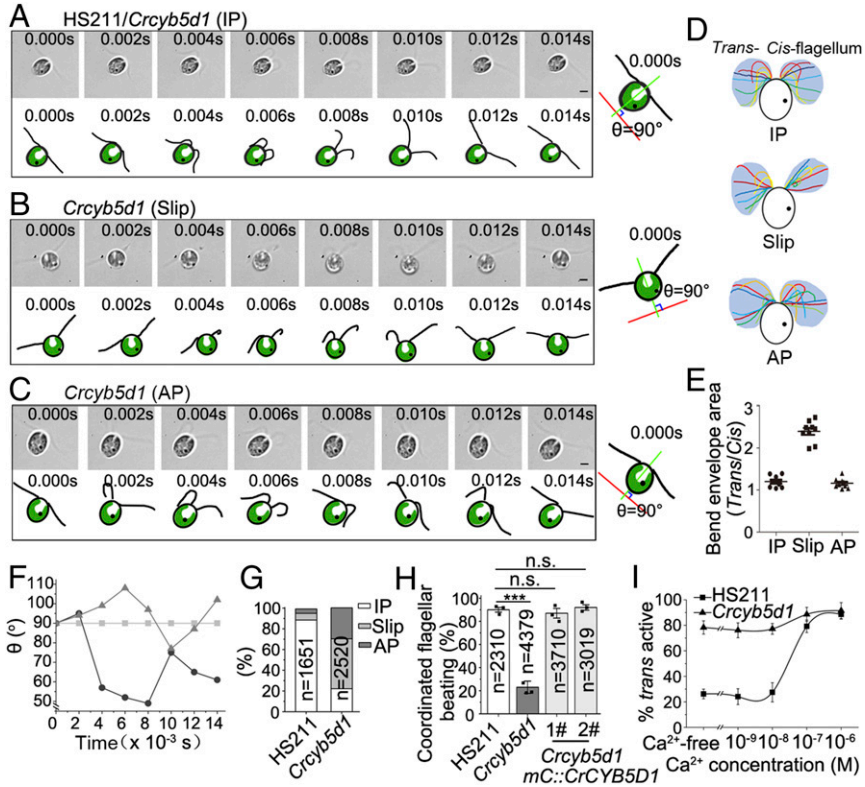

Fig. 3. CrCYB5D1 is responsible for controlling cis–trans flagellar dominance. Real-time images and schematic diagrams of the flagellar beat waveforms in IP (HS211 or *Crcyb5d1*) (*A*), Slip (*Crcyb5d1*) (*B*), and AP (*Crcyb5d1*) (*C*) states: IP, in-phase; Slip, phase slip; AP, antiphase. The schematic diagrams at right show the principle for comparing the waveforms of cis- and trans-flagella using the rotating angle of the cell body. The green line was set between the base of the two flagella, bisects the cell body, and changed over time. The red line is perpendicular to the green line at 0.000 s and was fixed during the analysis. The angle (θ) between the red and green lines was used to monitor the rotation of the cell body and was 90° at 0.000 s. Images were taken at 500 frames per second using a high-speed video microscopy. The time of each image is indicated. (Scale bars, 5 μm.) (*D*) Typical sequential flagellar bending patterns in a single beat cycle were reconstructed from the waveforms in *A*, *B*, and *C*. (*E*) Dot graph showing the ratio of bend envelope area between the trans- and cis-flagellum. All values are shown as the mean ± SD. (*F*) Comparing the angle (θ) of each beating waveform over time in HS211 and *Crcybd51*: IP, Box-marked line; AP, Triangle-marked line; Slip, Round-marked line. (*G*) Comparison of the percentage of IP, Slip, and AP states in beat cycles of HS211 and *Crcyb5d1*. The number of cycles is indicated. (*H*) Percentage of coordinated beat cycles in the indicated strains. All values are shown as the mean ± SEM of three independent experiments. ***$P < 0.001$. (*I*) The effect of Ca^{2+} concentration on the dominance of cis- and trans-axonemes in HS211 and *Crcybd51*. Each point shows the average and the SD from three experiments. The number of cells counted in each experiment was larger than 150.

flagella of *pf14* (Fig. 5*B*), indicating that CrCYB5D1 is localized to the stalk. In addition, immunogold-labeled flagella showed that 64% of gold particles were distributed along the stalk of the radial spokes in flagella of *Crcyb5d1 mC::CrCYB5D1*; in contrast, only a few gold particles were observed in the *Crcyb5d1* flagella and were distributed randomly (Fig. 5 *C* and *D*). These results demonstrate that CrCYB5D1 is located in the stalk of the radial spoke.

To further confirm that CrCYB5D1 is a radial spoke stalk protein, fractions enriched in radial spoke complexes from HS211 and *Crcyb5d1* were prepared by sequential 0.6 M NaCl and 0.5 M KI extractions (39) and proteins present in the 0.5 M KI extract were compared using mass spectrometry. All the previously known radial spoke components as well as CrCYB5D1 were identified in flagella of HS211 (*SI Appendix*, Table S1). However, CrCYB5D1, along with RSP20 and RSP12 were not found in flagella of *Crcyb5d1*, whereas all other radial spoke proteins were identified, with an abundance ratio of these proteins in the two strains close to 1 (*SI Appendix*, Table S1). These data confirm that CrCYB5D1 is a component of the radial spoke stalk and suggest that it may associate with and affect the incorporation of RSP20 and RSP12. This speculation is supported by the recently published radial spoke structural model in which CrCYB5D1 interacts with RSP12 spatially (40).

The radial spoke complex first assembles into a "7"- or "L" -shaped 12S precursor in the cell body and is then incorporated into the axoneme as a mature T-shaped 20S spoke (41, 42). To determine when CrCYB5D1 was incorporated into the radial spokes, a whole-cell lysate of *Crcyb5d1 mC::CrCYB5D1* was fractionated by sucrose density gradient centrifugation. The majority of mC::CrCYB5D1 sedimented at 6S and 20S. In contrast, RSP1 and RSP2 signals peaked at 6S, 20S, and 12S (Fig. 5*E*), which is characteristic of most radial spoke proteins in sucrose density gradients. 20S complexes in the cytoplasm come from the disassembly of flagella during the cell cycle, whereas the 12S complexes are strictly preassembly forms (43). CrCYB5D1 cosedimented with RSP1 and RSP2 only at 20S, but not 12S, indicating that the assembly of CrCYB5D1 into the mature radial spokes is independent of the 12S precursor. To further confirm this conclusion, the membrane plus matrix of isolated flagella from *Crcyb5d1 mC::CrCYB5D1* cells was fractionated using sucrose density gradient centrifugation. We found that CrCYB5D1 also cosedimented with RSP1 and RSP2 only at 20S, but not 12S (Fig. 5*F*), confirming that the assembly of CrCYB5D1 into the mature radial spokes is independent of the 12S precursor. Thus, CrCYB5D1 may be transported into flagella separately.

A cell lysate of *Crcyb5d1* was also fractionated in a sucrose density gradient; immunoblot analysis of each fraction revealed that RSP1 and RSP2 peaked at 6S, 12S, and 20S (*SI Appendix*, Fig. S9*A*), which was similar to the distribution of these proteins in *Crcyb5d1 mC::CrCYB5D1* cells (Fig. 5*E*). The amount of RSP1, RSP2, and RSP3 in flagella was similar in HS211, *Crcyb5d1,*

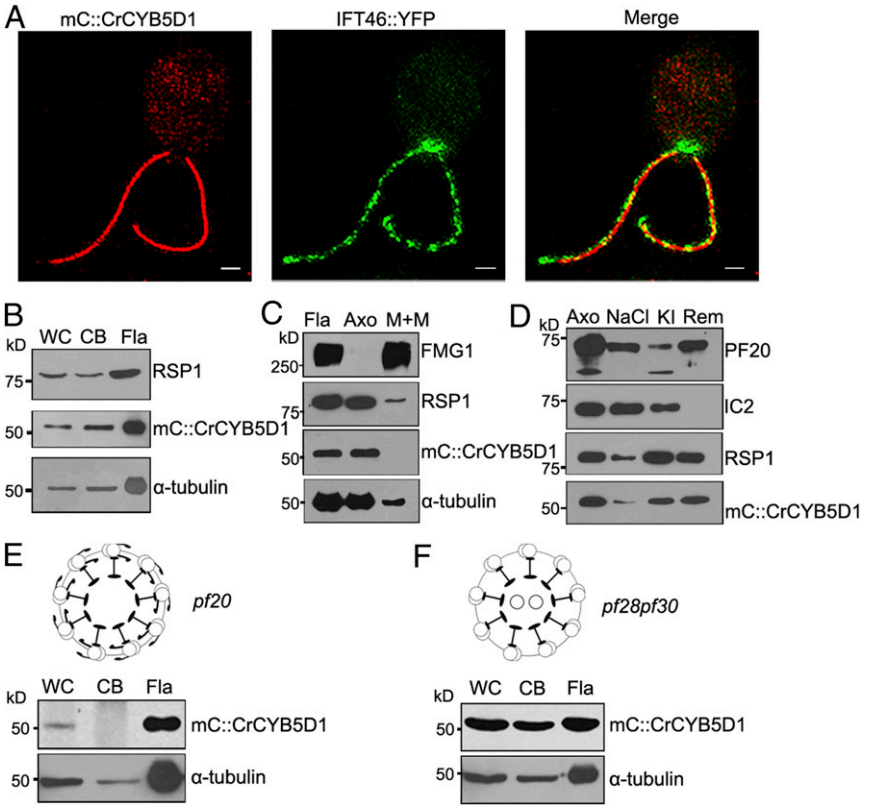

Fig. 4. CrCYB5D1 is a radial spoke protein. (*A*) Localization of mC::CrCYB5D1 and IFT46::YFP in the flagella of *Crcyb5d1 mC::CrCYB5D1* using 3D-SIM. (Scale bars, 2 μm.) (*B*) Immunoblot analysis of equal amounts of protein from whole-cells (WC), cell bodies (CB), and isolated flagella (Fla) of *Crcyb5d1 mC::CrCYB5D1* probed with antibodies against RSP1, mCherry, and α-tubulin. (*C*) Immunoblot analysis of flagella, axonemes, and membrane plus matrix isolated from *Crcyb5d1 mC::CrCYB5D1* probed with antibodies against FMG-1, RSP1, mCherry, and α-tubulin. FMG-1 is a flagellar membrane marker and RSP1 acts as a radial spoke marker. (*D*) Immunoblot analysis of a NaCl extract and subsequent KI extract of axonemes from *Crcyb5d1 mC::CrCYB5D1* probed with antibodies against PF20, IC2, RSP1, and mCherry. PF20 was used as a central pair marker and IC2 as an outer arm dynein marker. Immunoblot analysis of equal amounts of protein from whole-cells, cell bodies, and isolated flagella of *pf20 mC::CrCYB5D1* (*E*) and *pf28pf30 mC::CrCYB5D1* (*F*) probed with antibodies against mCherry and α-tubulin.

and *Crcyb5d1 mC::CrCYB5D1* strains (*SI Appendix*, Fig. S9*B*), which is consistent with the mass spectrometry results (*SI Appendix*, Table S1). The base, stalk, and head of the radial spokes in *Crcyb5d1* appeared normal under thin-section transmission EM and were indistinguishable from those in flagella of HS211 (*SI Appendix*, Fig. S9*C*). Collectively, these data suggest that CrCYB5D1 is not an essential structural component of the radial spoke complex, and its deficiency does not affect the assembly or gross organization of the radial spoke. Thus, it may play a regulatory role.

CrCYB5D1 Binds Heme. The Cyt-b5 domain at the N terminus of CYB5D1 potentially binds heme as it does in CYB5D2 (44). To test this hypothesis, an LC-MS/MS (liquid chromatography tandem mass spectrometry/mass spectrometry) method (45) was modified to determine the amount of heme in flagella. Heme was identified in flagella of both HS211 and *Crcyb5d1* (*SI Appendix*, Fig. S10); the heme concentration in *Crcyb5d1* flagella is $1.18 \pm 0.23 \times 10^{-10}$ mol heme/g flagella and in which HS211 flagella is $1.34 \pm 0.11 \times 10^{-10}$ mol heme/g flagella (Fig. 6*A*). These results suggested the presence of heme-binding proteins in flagella and that CrCYB5D1 may be one of them.

Subsequently, a whole-cell lysate of HS211 expressing CrCYB5D1::-Strep was incubated with hemin–agarose (hemin is heme containing ferric iron with coordinated chloride), and hemin-bound proteins were eluted with Tris buffer containing SDS and β-mercaptoethanol. Immunoblot analysis revealed that about 90% of CrCYB5D1::Strep adhered to the hemin–agarose (Fig. 6*B*). To further confirm this, freshly purified CrCYB5D1::Strep was incubated with hemin–agarose; about 80% CrCYB5D1::Strep adhered to the hemin–agarose (Fig. 6*C*). Hemin exhibits a maximum absorbance (A_{max}) at 382 nm (Fig. 6*D* red line). When CYB5D1 was added to the hemin solution, the A_{max} shifted to 402 nm (Fig. 6*D*, green line), which is a typical characteristic of heme-binding proteins (44, 46). Then, increasing concentrations of hemin were added to a fixed concentration (3 μM) of CrCYB5D1. When the molar ratio of hemin to CrCYB5D1 reached 1:1, the absorption increasement at 402 nm plateaued (Fig. 6*E*). Thus, CrCYB5D1 binding to hemin is saturable and occurs at a 1:1 stoichiometry.

Heme Binding by CrCYB5D1 Is Redox Sensitive. CrCYB5D1 contains four cysteine residues (amino acids 26, 76, 101, and 147) that may form disulfide bonds and affect heme-binding. To determine whether the thiols present in CrCYB5D1 were in reduced or oxidized form, 4-acetamido-4-maleimidylstilbene-2,2′-disulfonic acid (AMS), which reacts only with reduced thiols and adds 490 Da per modified thiol, was used (21). Purified CrCYB5D1::Strep from whole cells was incubated in an oxidizing buffer containing GSSG (oxidized glutathione), reducing buffer containing DTT (dithiothreitol), or Tris buffer without any redox reagents (NT) for 30 min, and then fixed with TCA (trichloroacetic acid). Subsequently, reduced thiol groups were alkylated with AMS. Immunoblot analysis revealed that most of CrCYB5D1 was in an oxidized state following GSSG treatment, while DTT treatment fully reduced CrCYB5D1.

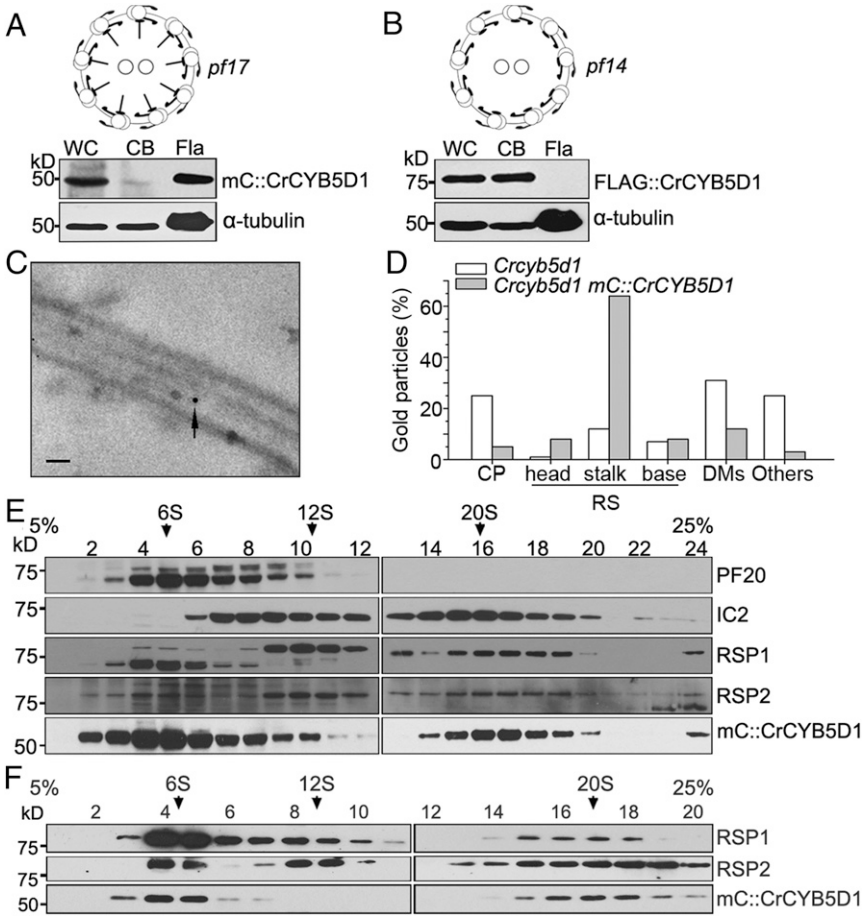

Fig. 5. CrCYB5D1 localizes to the radial spoke stalk. Immunoblot analysis of equal amounts of protein from whole-cells, cell bodies, and isolated flagella of strains *pf17 mC::CrCYB5D1* (*A*) and *pf14 FLAG::CrCYB5D1* (*B*) probed with antibodies against mCherry and FLAG, respectively. (*C*) Representative immunogold electron micrograph of CrCYB5D1 localized at the stalk of the flagellar radial spoke using anti-mCherry antibody and a gold-conjugated secondary antibody. (Scale bar, 100 nm.) (*D*) The percentage of gold particles localized to different axoneme-associated components including the central pair (CP), radial spoke (RS) head, stalk and base, and the doublet microtubules (DMs). (*E*) Proteins from a whole-cell lysate of *Crcyb5d1 mC::CrCYB5D1* were separated using sucrose density gradient centrifugation and collected in 24 fractions. Each fraction was subject to immunoblot analysis using antibodies against PF20, IC2, RSP1, RSP2, and mCherry. (*F*) Proteins from a flagellar membrane-matrix fraction of *Crcyb5d1 mC::CrCYB5D1* were separated using sucrose density gradient centrifugation and collected in 20 fractions. Each fraction was subject to immunoblot analysis using antibodies against RSP1, RSP2, and mCherry.

The purified untreated CrCYB5D1 sample contained about 50% oxidized form in vitro (Fig. 6*F* and *SI Appendix*, Fig. S11*A*). These results suggest that purified CrCYB5D1 contains at least one reduced and one oxidized form.

To determine which form of CrCYB5D1 binds heme, purified CrCYB5D1::Strep was first treated with or without DTT and then incubated with hemin. Since hemin promotes the peroxidase reaction, if a protein binds hemin, a chemiluminescent signal will appear at the location of this protein band on the PVDF (polyvinylidene fluoride) membrane. Signal was only detected in CrCYB5D1 samples that had not been treated with DTT (Fig. 6*H*, lane 4), indicating that only the oxidized form of CrCYB5D1 binds heme groups specifically.

Redox Regulates the Coordinated Flagellar Beating. To determine whether CrCYB5D1 in flagella also has reduced and oxidized forms, flagella from HS211 cells expressing CrCYB5D1::Strep were isolated and treated with DTT or H_2O_2 for 1 min, and the redox state of CrCYB5D1 was determined using the AMS labeling assay. The ratio of reduced to oxidized CrCYB5D1 was about 19:1 in flagella without any treatment. DTT treatment resulted in more reduced CrCYB5D1, and the ratio increased to 33:1; in contrast, H_2O_2 treatment increased the oxidized form of CrCYB5D1 and the ratio decreased to 10:1 (Fig. 7*A* and *SI Appendix*, Fig. S11*B*).

Since there are four cysteines in CrCYB5D1, parallel reaction monitoring (PRM) mass spectrometry was used to determine which two of them can form a disulfide bond in flagella. The disulfide bond between C26 and C76 was detected in untreated flagella. In DTT-treated flagella, an additional disulfide bond between C101 and C147 was found. In H_2O_2-treated isolated flagella, a third disulfide bond between C76 and C101 was detected (Fig. 7*B* and *SI Appendix*, Fig. S12). The Peptide-Spectrum Matches (PSMs) number increased to 9 in the H_2O_2-treated flagella from 5 in NT flagella when the same amount of protein was used for analysis, which is consistent with the AMS-labeling result (Fig. 7*A*). CrCYB5D1 from H_2O_2-treated or nontreated flagella could be purified on hemin–agarose; in contrast, CrCYB5D1 could not be purified from DTT-treated flagella (Fig. 7*C*). These results suggest that at least two forms of CrCYB5D1 exist in flagella—oxidized (heme-binding) and reduced (non-heme-binding)—and their dynamic balance can be modulated by environmental factors.

Since the binding of heme to CrCYB5D1 is redox dependent, defects in coordinated flagellar beating in the *Crcyb5d1* strain may be due to alterations in flagellar redox state. To test this hypothesis, we used a redox-sensitive outer arm dynein component

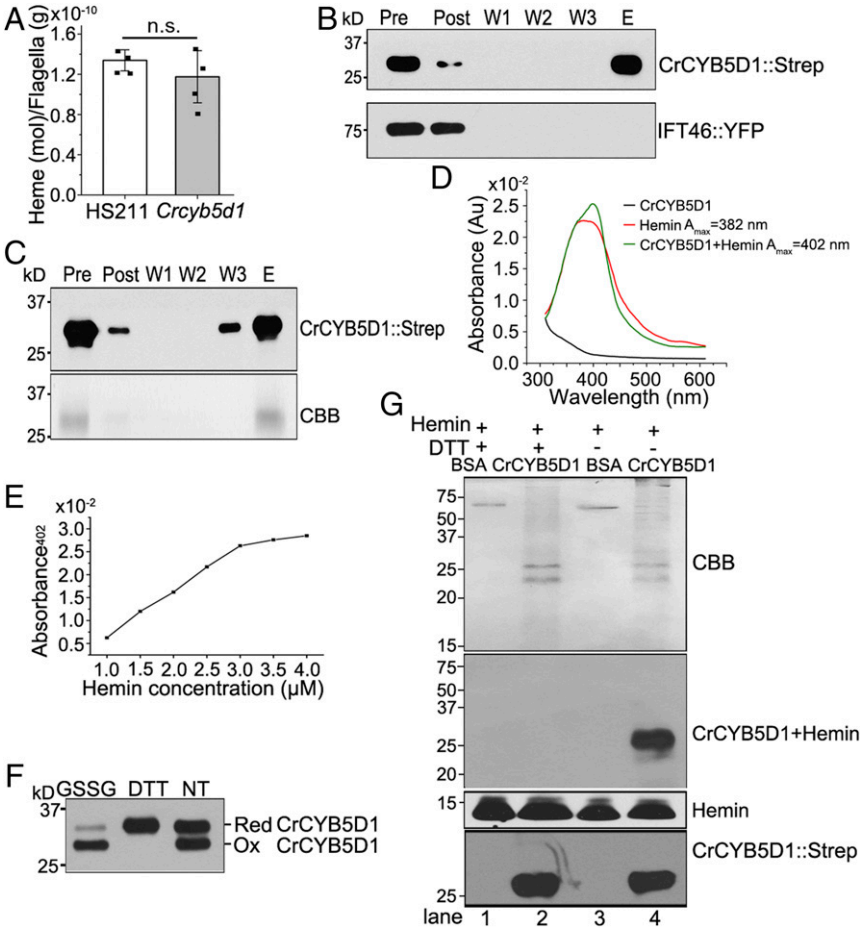

Fig. 6. CrCYB5D1 binds heme in a redox-sensitive manner. (*A*) Comparison of the heme concentration in flagella of HS211 and *Crcyb5d1*. All values are shown as the mean ± SD of four independent experiments. n.s., not significant. Immunoblot analysis of the binding activity of CrCYB5D1::Strep from whole-cell lysate (*B*) or freshly purified CrCYB5D1::Strep (*C*) from HS211 cells expressing CrCYB5D1::Strep using hemin-conjugated agarose and an anti-Strep antibody (*Upper*); IFT46::YFP is a negative control in *B*. In *C*, the total protein was assessed by Coomassie blue staining (CBB, *Lower*). "Pre," the soluble fraction of the cell lysate before incubation with hemin-conjugated agarose beads; "Post," the soluble fraction after incubation with hemin-conjugated agarose beads; "W1," "W2," and "W3," wash fractions; "E," the bound fraction eluted with SDS and β-mercaptoethanol. (*D*) The absorbance spectra between 300 and 600 nm were collected for 3 μM CrCYB5D1::Strep, 50 μM hemin, and 50 μM hemin mixed with 3 μM CrCYB5D1::Strep. (*E*) The maximum absorbance (A_{max}) at 402 nm resulting from heme binding to CrCYB5D1::Strep was plotted for a concentration series of hemin mixed with 3 μM CrCYB5D1::Strep. (*F*) Assessment of the redox state of purified CrCYB5D1::Strep from whole cells. 50 mM GSSG or 1 mM DTT were used as oxidative and reductive treatments, respectively; NT indicates no treatment. The quantitative ratio of reduced and oxidized CrCYB5D1 in *F* under different conditions (see main text) was determined by immunoblot analysis. (*G*) Detection of heme-promoted peroxidase activity using purified CrCYB5D1::Strep. The top shows Coomassie blue staining; the second panel indicates peroxidase activity of the CrCYB5D1–hemin complex; the third panel shows peroxidase activity with free hemin, and the bottom shows immunoblot analysis of samples probed with Strep antibody.

LC3 as a marker to compare the redox state in flagella of HS211 and *Crcyb5d1*. Oxidized and reduced LC3 are present in flagella, and the reduced form generally predominates (21). The flagella of HS211 and *Crcyb5d1* cells were isolated after treated with 1 mM DTT and 1 mM H_2O_2 for 1 min and alkylated with AMS. Immunoblot analysis of these samples with LC3 antibody showed that LC3 was nearly fully reduced in the flagella from HS211 and *Crcyb5d1*, or DTT-treated HS211 and *Crcyb5d1*. When the cells were treated with H_2O_2, the ratio of reduced versus oxidized LC3 was 1.3:1 in flagella of HS211, but 1.8:1 in flagella of *Crcyb5d1* (Fig. 7*D* and *SI Appendix*, Fig. S11*C*), suggesting that the redox state of *Crcyb5d1* flagella is more reductive than in HS211.

To determine whether this enhanced reductive state resulted in uncoordinated flagellar beating, the flagellar waveforms of HS211 and *Crcyb5d1* cells were compared after treatment with the reducing agents DTT and membrane-permeable 4-hydroxy-2,2,6,6-tetramethylpiperidine 1-oxyl (TEMPOL) or with the oxidizing agents H_2O_2 and tertiary butyl hydroperoxide (t-BOOH) (21, 47, 48). The percentage of coordinated flagellar beating in HS211 decreased after 1 mM DTT (Movie S9) and 40 mM TEMPOL treatments (Movie S11) (Fig. 7*E*); in contrast, the low level of flagellar coordination in *Crcyb5d1* was unaffected (Fig. 7*F* and Movies S10 and S12). Interestingly, the percentage of *Crcyb5d1* coordinated flagellar beating increased following treatment with 2 mM H_2O_2 (Movie S14) and 0.5 mM *t*-BOOH (Movie S16) (Fig. 7*F*), but there was no effect when HS211 cells were treated with H_2O_2/*t*-BOOH (Movies S13 and S15) (Fig. 7*E*). Thus, the uncoordinated flagellar beating in *Crcyb5d1* cells could be mimicked by the treatment of HS211 cells with reducing agents. Furthermore, coordinated beating could be restored in *Crcyb5d1* cells by treating them with oxidizing agents. Taken together, these results suggest that flagellar redox state modulates coordinated beating.

The effect of redox state on flagellar beat frequency was also analyzed. Treatment with the reductants DTT or TEMPOL did not change the beat frequency of either HS211 or *Crcyb5d1* (*SI Appendix*, Fig. S13). Similarly, *t*-BOOH treatment also did not affect the beat frequency of either strain (*SI Appendix*, Fig. S13). However, H_2O_2 treatment decreased the beat frequency in both

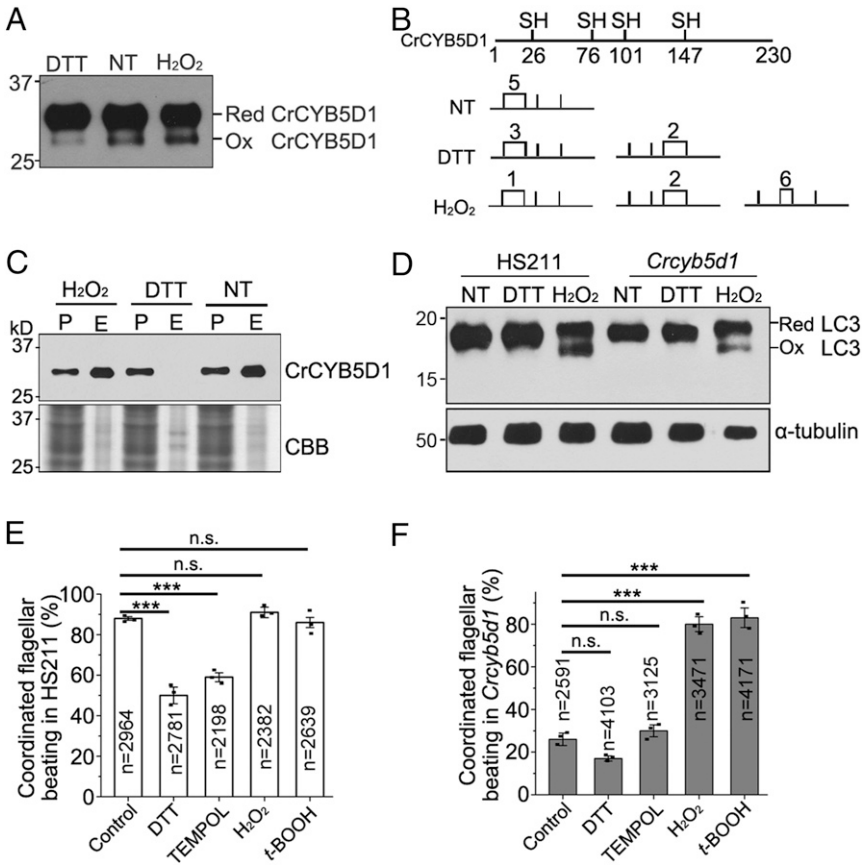

Fig. 7. CrCYB5D1 participates in redox-dependent regulation of coordinated flagellar beating. (*A*) Assessment of the redox state of CrCYB5D1::Strep in isolated flagella treated with 1 mM H_2O_2 or 1 mM DTT; NT indicates no treatment. (*B*) Summary of identified disulfide bonds from the samples in *A* by PRM MS. The number of peptide spectral matches (PSMs) are indicated. (*C*) Comparison of heme-binding activity of CrCYB5D1::Strep from the flagella of DTT- or H_2O_2-treated cells using hemin-conjugated agarose;. NT indicates no treatment. "P," the soluble fraction of the flagella before incubation with hemin-conjugated agarose beads; "E," the bound fraction eluted with SDS and β-mercaptoethanol. (*D*) Immunoblot analysis of flagellar samples from HS211 and *Crcyb5d1* cells treated with 1 mM DTT or 1 mM H_2O_2 using antibody against outer arm dynein LC3; α-tubulin served as a loading control. (*E* and *F*) Percentage of HS211 and *Crcyb5d1* cells exhibiting coordinated flagellar beating upon treatment with 1 mM DTT, 40 mM TEMPOL, 0.5 mM *t*-BOOH, or 2 mM H_2O_2. The number of beat cycles is indicated. All values are shown as the mean ± SEM of three independent experiments. ***$P < 0.001$. n.s., not significant.

HS211 and *Crcyb5d1* (*SI Appendix*, Fig. S13). This likely reflects the higher concentration of H_2O_2 used compared to *t*-BOOH. As the decrease in flagellar beat frequency was similar in both strains, changes in frequency are not responsible for the rescue of the uncoordinated beating phenotype in *Crcyb5d1*.

Flagellar coordination is tightly coupled to the phototaxis pathway (19), which is also regulated by redox (22). To determine whether the change of redox state in flagella of *Crcyb5d1* also affected phototaxis, low intensity (~1 μmol photon · m^{-2} · s^{-1}) or high intensity (10 μmol photons m^{-2} · s^{-1}) green LED light was used in a phototaxis assay as described previously (22). Both HS211 and *Crcyb5d1* cells showed positive phototaxis under low intensity light and negative phototaxis under high intensity light; however, in both cases, the *Crcyb5d1* mutant accumulated more slowly compared to HS211 (*SI Appendix*, Fig. S14 *A* and *B*). When the cells of HS211 and *Crcyb5d1* were treated with oxidizing agents, both cells exhibited positive phototaxis, and negative phototaxis was observed when cells were treated with reduced agents (*SI Appendix*, Fig. S14*C*), which agrees with the previous report (22). In both cases, *Crcyb5d1* phototaxis was slower compared to HS211; however, the phototactic defect in *Crcyb5d1* was partially rescued when cells were treated with oxidizing agents (*SI Appendix*, Fig. S14 *D* and *E*). This result suggests that the reductive shift in flagella of *Crcybd51* slows down phototaxis and that this slow down resulted from the increase in uncoordinated flagellar beating.

Discussion

In this study, we combined two classical ciliary research models, zebrafish and *Chlamydomonas*, to dissect the role of CYB5D1 in coordinated ciliary beating. CYB5D1 is a conserved radial spoke protein and located in the stalk of the radial spoke. In *Chlamydomonas*, disruption of CYB5D1 results in a beating defect of the cis-flagellum. Only the oxidized form of CYB5D1 can bind heme, which may regulate flagellar redox state and modulate the ciliary beating.

CYB5D1 Maintains the Flagellar Redox State through Binding Heme. Heme (iron–protoporphyrin IX) is a prosthetic group of hemoproteins. When it binds proteins, it performs a wide range of biological functions, including oxygen delivery, iron storage, electron transfer, and substrate oxidation (49). However, free heme, which has ferric iron bound, exerts redox toxicity in biological tissues mainly through the oxidative reactions of iron (50). Iron can cycle between ferrous and ferric states via Fenton chemistry and the Haber-Weiss reaction, yielding a regenerating supply of reactive oxygen species (ROS) (51). Our work reveals that heme is present in flagella (*SI Appendix*, Fig. S10) and can be used to generate ROS. ROS-generating enzymes such as nitric oxide synthase 1 (NOS1) (52) and dual oxidase 1 (DUOX1) (53) have also been characterized in motile cilia in mammals. Furthermore, ROS scavengers such as thioredoxins (Trxs), glutaredoxins (Gpxs), and peroxiredoxins

(Prxs) have been identified in flagella (25, 54, 55). Flagella of the *Crcyb5d1* mutant contains an amount of heme (Fig. 6*A*) and has a more reduced flagellar redox state as assessed using the redox-sensitive thioredoxin-like LC3 of outer arm dynein as a marker (Fig. 7*D* and *SI Appendix*, Fig. S11*C*). Thus, CYB5D1 may regulate the redox state of flagella by binding heme. Specifically, when ROS levels increase, the flagellar redox state would become more oxidative, leading to oxidation of CYB5D1 which can then bind free heme to decrease ROS levels. Conversely, when ROS decreases, the redox shifts to a more reductive state, CYB5D1 becomes reduced, releasing heme which can then generate ROS.

CYB5D1 May Integrate Environmental and Intraciliary Redox Signals to Coordinate Ciliary Beating. Flagellar motility is regulated by alterations in redox state (21), and flagella contain several motility-related redox-sensitive components. For example, the catalytic subunit C of protein phosphatase type 1 (PP1C) localizes to the central pair complex (56), and its activity can be enhanced by H_2O_2 (57). Protein phosphatase type 2A (PP2A) locates near inner dynein arm I1 and requires DTT for enzyme reactivation (57). Two subunits of the outer dynein arm (LC3 and LC5) contain thioredoxin redox-sensitive motifs and are specifically eluted from a phenylarsine oxide matrix with β-mercaptoethanol (25), while the outer arm docking complex protein DC3 is a redox-sensitive calmodulin homolog that binds calcium only in the reduced state (24). Furthermore, outer arm dynein ATPase activity is activated by sulfhydryl oxidation; this response is mediated through the γ-HC (26). A central pair protein (PF20), three radial spoke proteins (RSP1, RSP9, and RSP5), inner dynein arm subunits p28 (IDA4), actin (IDA5), the α (ODA11) and β (ODA4) HCs, and IC2 intermediate chain (ODA6) of the outer dynein arm have been identified in the thioredoxin interactome of *Chlamydomonas* (58); cells defective for these components exhibit altered swimming behavior (59–62). Collectively, these data suggest that these redox-related and/or redox-sensitive proteins may form a redox signaling pathway and regulate coordinated flagellar beating; CYB5D1 is an essential regulator of this pathway since it can sense and integrate environmental and intraciliary redox signals (Fig. 7 *A* and *B*).

However, how loss of CYB5D1 results in a waveform change in the cis-flagellum remains an unanswered question. Based on our data and published results, we propose a working model for redox control of coordinated ciliary beating. The redox state in the flagella of *Chlamydomonas* is relatively oxidizing, which is essential for the concerted activity of dyneins to coordinate beating of the two flagella; CrCYB5D1 is indispensable for maintaining this oxidative state by binding or releasing heme. When CrCYB5D1 is disrupted, the redox state in the trans and cis-flagella shift to a more reductive state (Fig. 7*D* and *SI Appendix*, Fig. S11*C*). If the cis-flagellum is more sensitive to this reductive state, a defective waveform would result and the coordination of flagellar beating lost in *Crcyb5d1* (Fig. 3). Reductant treatments also induced a reductive shift, so coordinated flagellar beating breaks down in wild type (Fig. 7*E*). When the redox state becomes more oxidizing in *Crcyb5d1* following oxidant treatment, the redox shift removes the defect in the cis-flagellum, and so coordinated beating is restored in *Crcybd51* (Fig. 7*F*). This model is based on the hypothesis that there is an asymmetry between the two flagella in which the cis-flagellum is more sensitive to reductant than the trans-flagellum. There are several lines to support such an asymmetry; the cis- and trans-flagellum have different sensitivities to calcium in vitro (19). The difference between the cis- and trans-flagellum beat frequencies is not observed in mutants lacking the outer arm docking complex (*oda1* and *oda3*) or in the *oda11* mutant lacking the outer dynein arm α heavy chain (63, 64). The defect in coordination of the trans and cis-flagella in *Crcybd51* is mainly due to changes in the intrinsic behavior of the cis-flagellum; the lack of coordinated beat is a secondary effect.

Calcium, Redox, and Phototaxis. The cis- and trans-axonemes of demembranated, reactivated wild type *Chlamydomonas* cell models respond differently to submicromolar levels of calcium: the cis-axoneme is more active at Ca^{2+} concentrations below 10^{-8} M, whereas the trans-axoneme was more active at higher Ca^{2+} concentrations (19). However, in the *Crcyb5d1* mutant, the trans-axoneme is constantly active and the cis-axoneme is inactive regardless of changes in the concentration of Ca^{2+}. This is different to the previously characterized mutants, *lsp1* and *ptx1*, in which the cis- and trans-axonemes are not sensitive to Ca^{2+} concentrations ranging from 0 to 10^{-6} M (65).

Mutants with defects in Ca^{2+}-dependent flagellar dominance such as *lsp1*, *ptx1*, and *Crcyb5d1* also show phototaxis defects (ref. 65 and this study). As an initial signal of phototaxis, light induces an inward current at the eyespot and depolarizes the membrane (66, 67), resulting in a Ca^{2+} influx and concomitant increase in intraflagellar Ca^{2+} concentration (68, 69). These data clearly demonstrated that Ca^{2+} play an important role in phototaxis. However, the sign of phototaxis (i.e., positive or negative) is regulated by redox. Cells always exhibited positive phototaxis after being treated with ROS and always displayed negative phototaxis after treatment with ROS quenchers (22). The positive phototaxis of *Crcybd51* was more defective than its negative phototaxis (*SI Appendix*, Fig. S14 *A* and *B*), which may result from a reductive shift in the flagella (Fig. 7*D*). These data further suggest that redox poise plays a critical role in controlling the direction of phototaxis.

Coordinated responses to changes in redox poise and Ca^{2+} may be mediated by differentially modifying the activity of the ODA in the cis- and trans-flagella, as the two flagella beat at almost the same frequency in cell models of the *oda1* mutant that lack the outer dynein arms (70). ODA light chains such as LC3 and LC5 are closely related to thioredoxin (25), and redox poise modulates the motility of flagella through the ODA during photokinesis (21). In addition, Ca^{2+} binding to LC4 changes the conformation of the N-terminal domain of the γ-HC and alters interactions between microtubules and the motor domain(s) of the outer dynein arm (71). Furthermore, the Ca^{2+}-binding loop of docking complex protein DC3 contains a vicinal dithiol, and only the reduced form can bind Ca^{2+} in vitro (62). Thus, outer dynein arms may integrate redox and Ca^{2+} signals (72), and mediate transitions between coordinated and uncoordinated beating of the two flagella during phototaxis.

In conclusion, we have described here CYB5D1 as a regulator of coordinated ciliary beating. It is a conserved radial spoke stalk protein that binds heme in a redox-sensitive manner. Our data suggest that intraciliary redox signaling and environmental signals are integrated by CYB5D1 to modulate coordinated ciliary beating. Several redox-related or redox proteins such as TXNDC3 and TXNDC6 have been identified as new PCD genes (28). As a newly identified redox protein, CrCYB5D1 is required for coordinated flagellar beating, and is conserved in humans (*SI Appendix*, Fig. S2). Thus, we suggest it be considered as a candidate PCD gene.

Materials and Methods

The full procedures for bioinformatic analysis; in situ hybridization and immunohistochemistry; zebrafish mutants and morpholinos; high-speed video microscopy of zebrafish; algal cell culture and strains; screening and rescue of the *Crcybd51* mutant; flagella isolation and fractionation; swimming track recording and assessment of swimming velocity; analysis of flagellar swimming behavior and beat frequency; SDS-PAGE and immunoblotting; sucrose density gradient centrifugation; superresolution microscopy (3D-SIM); electron microscopy and immunogold labeling; heme detection using LC-MS/MS; purification of CrCYB5D1; assay of hemin binding to CrCYB5D1; detection of heme-catalyzed peroxidase activity; assessment of the redox state of LC3 and CrCYB5D1 in flagella, phototaxis assays, cell model generation and reactivation; label-free mass spectrometry–based protein quantification; and assignment of the disulfide bonds by PRM mass spectrometry are provided in the *SI Appendix*.

Data Availability. All study data are included in the article and/or supporting information.

ACKNOWLEDGMENTS. This work was supported by the National Nature Science Foundation of China (Grant 31871358 to K.H. and 31400654 to G.L.) and the Strategic Priority Research Program of the Chinese Academy of Sciences (Grant No. XDPB18) to K.H. H.X., Y.K., and C.Z. were supported by the Marine S&T Fund of Shandong Province for the Pilot National Laboratory for Marine Science and Technology (Qingdao) (No. 2018SDKJ0406-2 to C.Z.) and the National Nature Science Foundation of China (Grant 31991194 to C.Z.); M.S.-A., R.S.P.-K., and S.M.K. were supported by grant GM051293 from the NIH (to S.M.K.). We thank Fang Zhou and Min Wang (Institute of Hydrobiology, Chinese Academy of Sciences) for cell imaging and LC-MS/MS analysis and Maya Yankova (Electron Microscopy Facility, University of Connecticut Health Center) for the immunogold electron microscopy. We thank Professor Joel Rosenbaum and Dr. Dennis Diener at Yale University, Professor Elizabeth Smith at Dartmouth College, and Professor Robert Bloodgood at the University of Virginia for sharing antibodies and Professor Deqiang Duanmu at Huazhong Agricultural University for providing plasmid pMD68.

1. W. Heydeck, L. Fievet, E. E. Davis, N. Katsanis, The complexity of the cilium: Spatiotemporal diversity of an ancient organelle. *Curr. Opin. Cell Biol.* **55**, 139–149 (2018).
2. K. H. Elliott, S. A. Brugmann, Sending mixed signals: Cilia-dependent signaling during development and disease. *Dev. Biol.* **447**, 28–41 (2019).
3. A. Meunier, J. Azimzadeh, Multiciliated cells in animals. *Cold Spring Harb. Perspect. Biol.* **8**, a028233 (2016).
4. C. Kempeneers, M. A. Chilvers, To beat, or not to beat, that is question! The spectrum of ciliopathies. *Pediatr. Pulmonol.* **53**, 1122–1129 (2018).
5. S. M. King, Axonemal dynein arms. *Cold Spring Harb. Perspect. Biol.* **8**, a028100 (2016).
6. J. Lin, D. Nicastro, Asymmetric distribution and spatial switching of dynein activity generates ciliary motility. *Science* **360**, 396 (2018).
7. P. Rompolas, R. S. Patel-King, S. M. King, An outer arm Dynein conformational switch is required for metachronal synchrony of motile cilia in planaria. *Mol. Biol. Cell* **21**, 3669–3679 (2010).
8. I. H. Riedel, K. Kruse, J. Howard, A self-organized vortex array of hydrodynamically entrained sperm cells. *Science* **309**, 300–303 (2005).
9. K. Kunimoto *et al*., Coordinated ciliary beating requires Odf2-mediated polarization of basal bodies *via* basal feet. *Cell* **148**, 189–200 (2012).
10. K. Y. Wan, R. E. Goldstein, Coordinated beating of algal flagella is mediated by basal coupling. *Proc. Natl. Acad. Sci. U.S.A.* **113**, E2784–E2793 (2016).
11. N. Narematsu, R. Quek, K. H. Chiam, Y. Iwadate, Ciliary metachronal wave propagation on the compliant surface of *Paramecium* cells. *Cytoskeleton (Hoboken)* **72**, 633–646 (2015).
12. H. Wu *et al*., Solution structure of a dynein motor domain associated light chain. *Nat. Struct. Biol.* **7**, 575–579 (2000).
13. M. Ichikawa *et al*., Axonemal dynein light chain-1 locates at the microtubule-binding domain of the γ heavy chain. *Mol. Biol. Cell* **26**, 4236–4247 (2015).
14. R. S. Patel-King, S. M. King, An outer arm dynein light chain acts in a conformational switch for flagellar motility. *J. Cell Biol.* **186**, 283–295 (2009).
15. A. Toda, Y. Nishikawa, H. Tanaka, T. Yagi, G. Kurisu, The complex of outer-arm dynein light chain-1 and the microtubule-binding domain of the γ heavy chain shows how axonemal dynein tunes ciliary beating. *J. Biol. Chem.* **295**, 3982–3989 (2020).
16. P. Urbanska *et al*., The CSC proteins FAP61 and FAP251 build the basal substructures of radial spoke 3 in cilia. *Mol. Biol. Cell* **26**, 1463–1475 (2015).
17. E. E. Dymek, T. Heuser, D. Nicastro, E. F. Smith, The CSC is required for complete radial spoke assembly and wild-type ciliary motility. *Mol. Biol. Cell* **22**, 2520–2531 (2011).
18. C. G. DiPetrillo, E. F. Smith, Pcdp1 is a central apparatus protein that binds $Ca^{(2+)}$-calmodulin and regulates ciliary motility. *J. Cell Biol.* **189**, 601–612 (2010).
19. R. Kamiya, G. B. Witman, Submicromolar levels of calcium control the balance of beating between the two flagella in demembranated models of *Chlamydomonas*. *J. Cell Biol.* **98**, 97–107 (1984).
20. R. Kamiya, M. Okamoto, A mutant of *Chlamydomonas reinhardtii* that lacks the flagellar outer dynein arm but can swim. *J. Cell Sci.* **74**, 181–191 (1985).
21. K. Wakabayashi, S. M. King, Modulation of *Chlamydomonas reinhardtii* flagellar motility by redox poise. *J. Cell Biol.* **173**, 743–754 (2006).
22. K. Wakabayashi, Y. Misawa, S. Mochiji, R. Kamiya, Reduction-oxidation poise regulates the sign of phototaxis in *Chlamydomonas reinhardtii*. *Proc. Natl. Acad. Sci. U.S.A.* **108**, 11280–11284 (2011).
23. A. Honda *et al*., Effects of hydrogen peroxide on mucociliary transport in human airway epithelial cells. *Toxicol. Mech. Methods* **24**, 191–195 (2014).
24. D. M. Casey, T. Yagi, R. Kamiya, G. B. Witman, DC3, the smallest subunit of the *Chlamydomonas* flagellar outer dynein arm-docking complex, is a redox-sensitive calcium-binding protein. *J. Biol. Chem.* **278**, 42652–42659 (2003).
25. R. S. Patel-King, S. E. Benashki, A. Harrison, S. M. King, Two functional thioredoxins containg redox-senesitive vicinal dithiols from the Chlamydomonas outer dynein arm. *J. Biol. Chem.* **271**, 6283–6291 (1996).
26. A. Harrison *et al*., Redox-based control of the gamma heavy chain ATPase from *Chlamydomonas* outer arm dynein. *Cell Motil. Cytoskeleton* **52**, 131–143 (2002).
27. C. M. Sadek *et al*., Characterization of human thioredoxin-like 2. A novel microtubule-binding thioredoxin expressed predominantly in the cilia of lung airway epithelium and spermatid manchette and axoneme. *J. Biol. Chem.* **278**, 13133–13142 (2003).
28. B. Duriez *et al*., A common variant in combination with a nonsense mutation in a member of the thioredoxin family causes primary ciliary dyskinesia. *Proc. Natl. Acad. Sci. U.S.A.* **104**, 3336–3341 (2007).
29. B. B. Riley, C. Zhu, C. Janetopoulos, K. J. Aufderheide, A critical period of ear development controlled by distinct populations of ciliated cells in the zebrafish. *Dev. Biol.* **191**, 191–201 (1997).
30. X. Cheng *et al*., Building a multipurpose insertional mutant library for forward and reverse genetics in *Chlamydomonas*. *Plant Methods* **13**, 36 (2017).
31. K. C. Leptos *et al*., Antiphase synchronization in a flagellar-dominance mutant of *Chlamydomonas*. *Phys. Rev. Lett.* **111**, 158101 (2013).
32. K. Y. Wan, K. C. Leptos, R. E. Goldstein, Lag, lock, sync, slip: The many 'phases' of coupled flagella. *J. R. Soc. Interface* **11**, 20131160 (2014).
33. U. Ruffer, W. Nultsch, High-speed cinematographic analysis of the movement of *Chlamydomonas*. *Cell Motil.* **5**, 251–263 (1985).
34. B. Lv *et al*., Intraflagellar transport protein IFT52 recruits IFT46 to the basal body and flagella. *J. Cell Sci.* **130**, 1662–1674 (2017).
35. E. F. Smith, P. A. Lefebvre, PF20 gene product contains WD repeats and localizes to the intermicrotubule bridges in *Chlamydomonas* flagella. *Mol. Biol. Cell* **8**, 455–467 (1997).
36. G. Piperno, Z. Ramanis, E. F. Smith, W. S. Sale, Three distinct inner dynein arms in *Chlamydomonas* flagella: Molecular composition and location in the axoneme. *J. Cell Biol.* **110**, 379–389 (1990).
37. B. Huang, G. Piperno, Z. Ramanis, D. J. Luck, Radial spokes of *Chlamydomonas* flagella: Genetic analysis of assembly and function. *J. Cell Biol.* **88**, 80–88 (1981).
38. G. Piperno, B. Huang, Z. Ramanis, D. J. Luck, Radial spokes of *Chlamydomonas* flagella: Polypeptide composition and phosphorylation of stalk components. *J. Cell Biol.* **88**, 73–79 (1981).
39. P. Yang, D. R. Diener, J. L. Rosenbaum, W. S. Sale, Localization of calmodulin and dynein light chain LC8 in flagellar radial spokes. *J. Cell Biol.* **153**, 1315–1326 (2001).
40. M. Gui *et al*., Structures of radial spokes and associated complexes important for ciliary motility. *Nat. Struct. Mol. Biol.* **28**, 29–37 (2021).
41. D. R. Diener *et al*., Sequential assembly of flagellar radial spokes. *Cytoskeleton (Hoboken)* **68**, 389–400 (2011).
42. K. F. Lechtreck, I. Mengoni, B. Okivie, K. B. Hilderhoff, *In vivo* analyses of radial spoke transport, assembly, repair and maintenance. *Cytoskeleton (Hoboken)* **75**, 352–362 (2018).
43. H. Qin, D. R. Diener, S. Geimer, D. G. Cole, J. L. Rosenbaum, Intraflagellar transport (IFT) cargo: IFT transports flagellar precursors to the tip and turnover products to the cell body. *J. Cell Biol.* **164**, 255–266 (2004).
44. A. Bruce, A. P. Rybak, CYB5D2 requires heme-binding to regulate HeLa cell growth and confer survival from chemotherapeutic agents. *PLoS One* **9**, e86435 (2014).
45. J. Fyrestam, C. Östman, Determination of heme in microorganisms using HPLC-MS/MS and cobalt(III) protoporphyrin IX inhibition of heme acquisition in *Escherichia coli*. *Anal. Bioanal. Chem.* **409**, 6999–7010 (2017).
46. I. Kimura *et al*., Neuferricin, a novel extracellular heme-binding protein, promotes neurogenesis. *J. Neurochem.* **112**, 1156–1167 (2010).
47. S. Mochiji, K. Wakabayashi, Redox regulation of phototactic migration in the green alga *Chlamydomonas reinhardtii* and its possible application. *Commun. Integr. Biol.* **5**, 196–198 (2012).
48. K. Sugiura, Y. Nishimaki, M. Owa, T. Hisabori, K. I. Wakabayashi, Assessment of the flagellar redox potential in *Chlamydomonas reinhardtii* using a redox-sensitive fluorescent protein, Oba-Qc. *Biochem. Biophys. Res. Commun.* **503**, 2083–2088 (2018).
49. J. M. Comer, L. Zhang, Experimental methods for studying cellular heme signaling. *Cells* **7**, 47 (2018).
50. S. Kumar, U. Bandyopadhyay, Free heme toxicity and its detoxification systems in human. *Toxicol. Lett.* **157**, 175–188 (2005).
51. R. L. Aft, G. C. Mueller, Hemin-mediated DNA strand scission. *J. Biol. Chem.* **258**, 12069–12072 (1983).
52. C. L. Jackson *et al*., Neuronal NOS localises to human airway cilia. *Nitric Oxide* **44**, 3–7 (2015).
53. M. X. Shao, J. A. Nadel, Dual oxidase 1-dependent MUC5AC mucin expression in cultured human airway epithelial cells. *Proc. Natl. Acad. Sci. U.S.A.* **102**, 767–772 (2005).
54. G. J. Pazour, N. Agrin, J. Leszyk, G. B. Witman, Proteomic analysis of a eukaryotic cilium. *J. Cell Biol.* **170**, 103–113 (2005).
55. K. Wakabayashi, S. M. King, Modulation of *Chlamydomonas reinhardtii* flagellar motility by redox poise. *J. Cell Biol.* **173**, 743–754 (2006).
56. P. Yang, L. Fox, R. J. Colbran, W. S. Sale, Protein phosphatases PP1 and PP2A are located in distinct positions in the *Chlamydomonas* flagellar axoneme. *J. Cell Sci.* **113**, 91–102 (2000).
57. D. Sommer, S. Coleman, S. A. Swanson, P. M. Stemmer, Differential susceptibilities of serine/threonine phosphatases to oxidative and nitrosative stress. *Arch. Biochem. Biophys.* **404**, 271–278 (2002).
58. M. E. Pérez-Pérez *et al*., The deep thioredoxome in *Chlamydomonas reinhardtii*: New insights into redox regulation. *Mol. Plant* **10**, 1107–1125 (2017).
59. D. R. Mitchell, Y. Kang, Identification of *oda6* as a *Chlamydomonas* dynein mutant by rescue with the wild-type gene. *J. Cell Biol.* **113**, 835–842 (1991).
60. M. LeDizet, G. Piperno, *ida4-1*, *ida4-2*, and *ida4-3* are intron splicing mutations affecting the locus encoding p28, a light chain of *Chlamydomonas* axonemal inner dynein arms. *Mol. Biol. Cell* **6**, 713–723 (1995).

61. T. Kato-Minoura, M. Hirono, R. Kamiya, *Chlamydomonas* inner-arm dynein mutant, *ida5*, has a mutation in an actin-encoding gene. *J. Cell Biol.* **137**, 649–656 (1997).
62. D. M. Casey *et al*., DC3, the 21-kDa subunit of the outer dynein arm-docking complex (ODA-DC), is a novel EF-hand protein important for assembly of both the outer arm and the ODA-DC. *Mol. Biol. Cell* **14**, 3650–3663 (2003).
63. H. Sakakibara, D. R. Mitchell, R. Kamiya, A *Chlamydomonas* outer arm dynein mutant missing the alpha heavy chain. *J. Cell Biol.* **113**, 615–622 (1991).
64. S. Takada, R. Kamiya, Beat frequency difference between the two flagella of *Chlamydomonas* depends on the attachment site of outer dynein arms on the outer-doublet microtubules. *Cell Motil. Cytoskeleton* **36**, 68–75 (1997).
65. N. Okita, N. Isogai, M. Hirono, R. Kamiya, K. Yoshimura, Phototactic activity in *Chlamydomonas* 'non-phototactic' mutants deficient in Ca^{2+}-dependent control of flagellar dominance or in inner-arm dynein. *J. Cell Sci.* **118**, 529–537 (2005).
66. H. Harz, P. Hegemann, Rhodopsin-regulated calcium currents in *Chlamydomonas*. *Nautre* **351**, 6 (1991).
67. F. F. Litvin, O. A. Sineshchekov, V. A. Sineshchekov, Photoreceptor electric potential in the phototaxis of the alga *Haematococcus pluvialis*. *Nature* **271**, 476–478 (1978).
68. C. Beck, R. Uhl, On the localization of voltage-sensitive calcium channels in the flagella of *Chlamydomonas reinhardtii*. *J. Cell Biol.* **125**, 1119–1125 (1994).
69. G. J. Pazour, O. A. Sineshchekov, G. B. Witman, Mutational analysis of the phototransduction pathway of *Chlamydomonas reinhardtii*. *J. Cell Biol.* **131**, 427–440 (1995).
70. H. Sakakibara, R. Kamiya, Functional recombination of outer dynein arms with outer arm-missing flagellar axonemes of a *Chlamydomonas* mutant. *J. Cell Sci.* **92**, 77–84 (1989).
71. M. Sakato, H. Sakakibara, S. M. King, *Chlamydomonas* outer arm dynein alters conformation in response to Ca^{2+}. *Mol. Biol. Cell* **18**, 3620–3634 (2007).
72. S. M. King, Turning dyneins off bends cilia. *Cytoskeleton (Hoboken)* **75**, 372–381 (2018).